Revista de Chimie
https://revistadechimie.ro
https://doi.org/10.37358/Rev. Chim.1949

Electrodeposited MnO_2-based Capacitive Composite Electrodes for Pb^{2+} Adsorption

TANG CHANG-BIN*, NIU HAO, LU YU-XUAN, WANG FEI, ZHANG YU-JIE, XUE JUAN-QIN
Xi'an University of Architecture and Technology, Xi'an, Shaanxi 710055, PR China

Abstract. *In order to effectively realize the removal of low concentrations of lead ions in wastewater via capacitive deionization technology, MnO_2 composite electrodes were prepared by a galvanostatic co-deposition approach, where polyaniline (PANI) and graphene were added to an MnO_2 deposition solution and nickel foam was chosen as the substrate of the electrode. The microstructure, capacitance characteristics and adsorption behavior of Pb^{2+} ions of the electrodes were analyzed by scanning electron microscopy, X-ray diffraction, X ray photoelectron spectroscopy, laser Raman spectroscopy, cyclic voltammetry and capacitance deionization processes. The experimental results showed that the MnO_2-PANI-graphene composite electrode has a high specific capacitance (132.8 F/g) and a 61.8% removal rate for simulated wastewater containing 20 mg/L Pb^{2+} ions under the conditions of 30°C and 1 mA/cm^2, with the addition of 1 g/L PANI and 3 g/L graphene, respectively. Electroadsorption process was in accordance with the Lagergren quasi-second-order kinetic equation. The co-deposition of PANI and graphene oxide could play obvious role in enhancing the adsorption capacity and stability of the electrodes.*

Keywords: *MnO_2-based capacitive composite electrodesm composite electrodepositionm Pb^{2+} ionsm electroadsorption*

1.Introduction

A large amount of wastewater containing Pb^{2+} is inevitably produced from non-ferrous metal mining and smelting [1–3], lead-acid batteries [4,5] and other chemical production processes [6]. Because of its non-degradability and the enrichment in natural circulation systems Pb^{2+} may cause serious harm to humans, animals and plants [7,8]. Therefore, the effective treatment of wastewater containing lead is an important and urgent issue for ecological security and the environment.

Compared with the current industrial main applications of ion exchange [9-11], chemical precipitation, physical/biological adsorption and other lead-containing wastewater treatment technologies, capacitive deionization (CDI) technology has some advantages, such as low energy consumption, high efficiency, environmental friendliness, simple operation, strong adaptability and so on, with broad application prospects for ion removal, including heavy metal ions [12,13]. CDI technology based on the principle of an electric double layer capacitor and a pseudocapacitor is an electrochemical controlled deionization method in which an external electric field (0.8–2.0 V) is applied to both electrodes to drive the charged ions to move towards the electrode with opposite charge to be adsorbed. When the adsorption achieves balance, the ions adsorbed on the electrode return to the solution to achieve the purpose of desorption through disconnecting the power supply or reversing the polarity of the applied power. The adsorption and desorption performance of CDI mainly relies on the physical and chemical properties of the electrode materials, which can directly determine the removal ability and electroadsorption efficiency of heavy metal ions. As a result, the preparation and application of electrode materials with high adsorption capacity are keys for the development of electroadsorption technology.

**email: tcbtop@126.com*

Graphite, activated carbon, carbon nanotubes (CNT), mesoporous carbon, ordered mesoporous carbon, graphene and other carbon material electrodes [14] have large specific surface areas and good conductivity but their double-layer capacitance and adsorption capacity are limited, their subsequent treatment is more complex and their costs are high. For this reason, metal oxide materials, such as MnO_2, with high Faraday pseudocapacitance are often selected. MnO_2 has the characteristics of a wide voltage window, a high theoretical specific capacitance (1380 F/g), rich reserves, low cost and good environmental compatibility. Moreover, MnO_2 can also react with water to produce a large number of hydroxyl groups and manganese minerals have strong adsorption capacity for heavy metal ions，especially for lead [15,16], so MnO_2 is expected to have a huge application value in the field of environmental engineering as a CDI electrode material. However, pure MnO_2 thin-coated electrodes generally have the disadvantages of large charge transfer resistance and low adsorption efficiency, which limit their application in the CDI process [17].

Three main strategies, namely, chemical doping [18,19], surface microstructure controlling [20,21] and compositing with other conductive materials [22-24], are commonly used to improve the adsorption performance of MnO_2 electrodes. Among them, the use of conductive material composites has proved to be one of the most effective approaches, therefore significant research has been focused on composite design and preparation [17]. manganese dioxide was electrodeposited on a carbon nanotube-chitosan composite to fabricate a MnO_2/CNT-CS composite electrode by Liu [25], that can achieve a specific capacitance of 42.3F/g at a sweep speed of 5mV/s, a removal capacity of 6.01 mg/g, and show good cycling performance, but low specific surface area results in lower adsorption capacity. Shi [26] prepared manganese oxide (MnO_x)-coated vertically aligned carbon nanotubes (VACNTs) via atomic layer deposition, which successfully achieved both a high load and a large specific surface area. The specific capacitance of the electrode material was 215±7 F/g at a 5 mV/s sweep speed and its adsorption capacity for Na^+ reached 490±30 μmol/g at 1.2 V, which is twice that of the original VACNTs. However, this electrode material is also difficult to apply commercially due to its high cost. Chen [27] synthesized poly(2-aminothiophenol) (PATP)/MnO_2 through in situ growth of MnO_2 nanoflakes on surfaces of PATP nanofibers and found the removal rate of 20 mg of adsorbent added into 20 mg/L lead ion solution was up to 99.5%, but its complex preparation process, inconvenient recovery and difficult subsequent regeneration hinder its practical use.

Based on the above research, considering the selection of conjugated polymer materials with good electrochemical performance and carbon materials with excellent conductivity as composite reinforcement materials, MnO_2 composite electrodes with excellent capacitance and adsorption performance can be obtained. Therefore, polyaniline (PANI) with a special P-electron structure and graphene with high specific surface area and conductivity were chosen as composite reinforcements in this study. Currently, the synthesis of MnO_2 with graphene and PANI as binary hybrids has been reported only in the field of energy and catalysis [24,28], with no research on the adsorption of heavy metal ions reported. In this study, foam nickel was chosen as the substrate and PANI and graphene were selected to enhance the comprehensive performance of MnO_2 electrodes by one-step electrodeposition. New composite binary MnO_2-PANI and ternary MnO_2-PANI-G capacitance electrode materials were prepared to achieve the effective adsorption of low concentration lead ions in wastewater.

2.Materials and methods

2.1 Materials and reagents

Nickel foam (380±20 g/wt.%, Taiyuan Li Yuan Company) was used as the base material of the electrode. PANI (Sinopharm Chemical Reagent Co., Ltd.), water soluble graphene (5 wt.%, Nanjing Xianfeng Nanometer Materials Technology Ltd.), manganese sulphate, hydrochloric acid and other reagents (Tianjin Fuchen Chemical Reagent Factory) were used as received to blend an electrodeposition bath solution in which deionized water was regarded as a solvent (resistivity of ~18.2 MΩcm) obtained through a Milli-Q system.

2.2 Fabrication of MnO_2 composite electrodes

The nickel foam with 1.5mm thickness was cut into 6 cm × 7 cm shapes, treated by acetone and 3 M hydrochloric acid washed to neutral by deionized water and then dried to constant weight at 60°C under a vacuum. A 0.1 M $MnSO_4$ solution is used as the basic formula of the electrodeposition bath. A certain amount of PANI and graphene nano-flake dispersion was selected as reinforcements of the composite deposition. The suspension solution was obtained by ultrasonic dispersion. MnO_2-based composite electrodes were anode electrodeposited at a current density of 1 mA/cm^2 at 30°C, with nickel foam and nickel plate used as the anode and cathode, respectively. Finally, composite electrodes were repeatedly washed with deionized water to remove the adhesion of the ions from the deposition solution and then dried for 6 h at 60°C in a vacuum. MnO_2-PANI electrodes were prepared by composite deposition with PANI particles and MnO_2-PANI-G electrodes were prepared by composite deposition with PANI particles and graphene nano-flake dispersion.

2.3 Microstructural characterization of MnO_2 composite electrodes

The microstructure of the electrodes was observed by field emission scanning electron microscopy (FESEM, Helios G4 CX FEI company). The phase composition of the electrodes was identified by an XRD-7000 Shimadzu X-ray diffractometer. The chemical composition of the electrode materials was analyzed by PHI5700 X-ray photoelectron spectroscopy (C1s calibration) with Al Kα X-rays as the excitation source and a Renishaw reflex confocal-micro Raman spectrometer.

2.4 Determining specific capacitance of electrodes

Cyclic voltammetry in 20 mg/L lead nitrate test solution was performed at a scan rate of 50 mV/s in the potential range of 0–1 V and in a three-electrode system in which the prepared electrodes were used as working electrodes, platinum plate was the counter electrode and saturated calomel was the reference electrode by employing a model PARSTAT4000 potentiostatic/galvanostatic instrument (Ametek, USA). According to the measured current-voltage curve, the corresponding specific capacitance of the electrodes was calculated by Eq. (1):

$$C = \frac{1}{2m \cdot v \cdot \Delta V} \int IdV \quad (1)$$

where C is the specific capacitance (F/g), M is the mass of the active substance (g), V is the scanning rate (mV/s), I is the current (A) and V is the scanning potential (V).

2.5 Electroadsorption characteristics and stability test

The CDI unit for the electroadsorption treatment (Figure 1), designed and assembled in our lab, consisted of an acrylic plate, a silica gel gasket, electrodes, a peristaltic pump, a DC power supply and a conductivity meter. The electroadsorption experiment was carried out in continuous inflow mode. First, 100 mL of distilled water was continuously pumped through the CDI unit by the peristaltic pump and then flowed out from the upper part, before being finally returned to the original solution beaker. When the conductivity of the outlet was stable, distilled water was replaced with 20 mg/L of solution containing lead ions at the intake. Subsequently, the voltage of 1.2 V is applied using the DC power supply at both electrodes (a composite electrode as the cathode and a blank nickel foam electrode as the anode) in the CDI unit. Electroadsorption experiments were carried out at room temperature (25°C). Finally, the conductivity of the solution no longer changed after a period of adsorption, the electroadsorption treatment was considered to reach equilibrium and the adsorption process is completed.

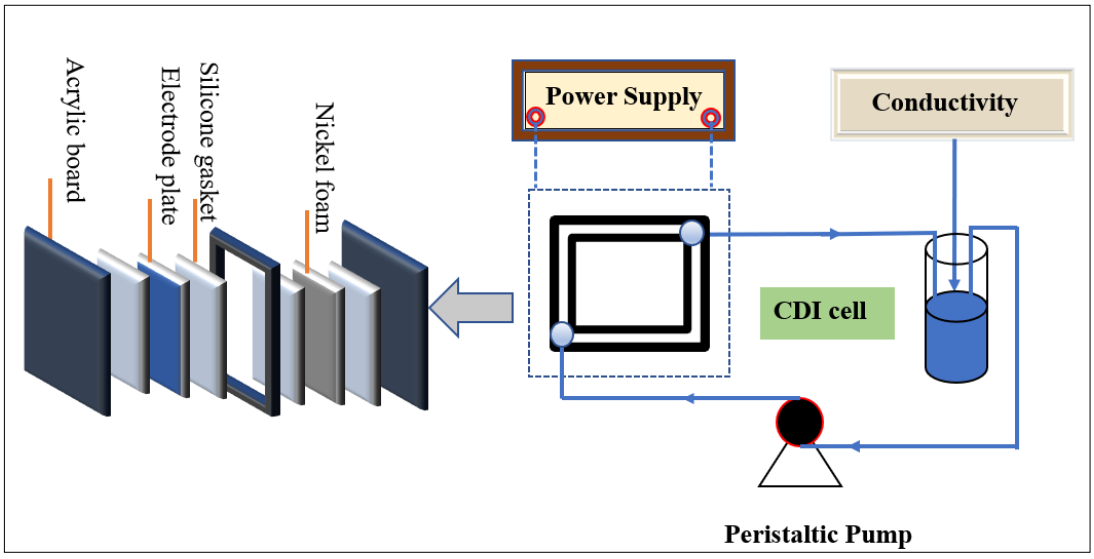

Figure 1. Schematic diagram of electrosorption experimental device

According to Eqs. (2) and (3), the removal efficiency (μ) and electroadsorption capacity (Q) of the electrode for Pb^{2+} ions are calculated, respectively:

$$\mu=\frac{c_0-c_t}{c_0}\times 100\% \quad (2)$$

$$Q_t=\frac{(c_0-c_t)V}{m} \quad (3)$$

where C_0 (mg/L) and C_t (mg/L) are the initial concentration of Pb^{2+} ions in the raw solution and its concentration at time t, respectively, V (L) is the volume of the Pb^{2+} ion solution, m (g) is the mass of the electrode and Q_t (mg/g) is the specific adsorption amount (i.e. electroadsorption capacity) at time t.

The adsorption stability of the composite electrodes was tested by the adsorption/desorption cycle process. After having finished adsorption and desorption for one cycle, the following adsorption and desorption cycle was conducted by using a fresh raw solution instead of the solution used in the previous experiment. Adsorption and desorption cycles were repeated three times. The stability of the electrode was evaluated by comparing the reduction of the removal efficiency of Pb^{2+} ions in each cycle.

3.Results and discussions

3.1 Microstructure of composite electrodes

Figure 2(a) shows the XRD spectrum of the MnO_2 and MnO_2-PANI-G composite electrodes. The diffraction peaks at 44.3° and 51.7° of 2θ correspond to the Ni phase, while the diffraction peaks at 76.2° of 2θ correspond to the γ-MnO_2 (450) crystal surface (JCPDS No.14-0644), illustrating that the XRD results mainly reflect the crystal structural information of the Ni substrate due to thin MnO_2 electrodeposited film. When PANI particles (1 g/L) and graphene nanosheet (3 g/L) were added to the deposition solution, the crystal structure of the composite electrodes is similar to the pure MnO_2 electrode; however, the half-width of the MnO_2 diffraction peak for the composite electrodes slightly increases, with broadening of the diffraction peak occurring, which indicated that the grain size decreased and the grains were refined due to co-deposition. The Raman spectra of the three electrodes are exhibited in Figure 2(b). It can be seen that the characteristic band centered at 260 and 298 cm^{-1} between 200 and 400 cm^{-1} should be assigned to the bending vibration of Mn-O-Mn in the MnO_2 lattice, and the two bands observed at 556 and 636 cm^{-1} between 500 and 700 cm^{-1} corresponded to the stretching vibration of Mn-O in the MnO_6 octahedra [29,30]. For the MnO_2-PANI and MnO_2-PANI-G electrodes, three Raman bands observed at 779, 1161 and 1491 cm^{-1}, corresponding to the deformation of the imino group in PANI, the in-plane bending of C-H bonds and the stretching vibration of C=N in the quinone ring, respectively, demonstrated that PANI obviously existed on the MnO_2 coating. The

characteristic bands of the MnO_2-PANI-G electrode at 1348 and 1580 cm^{-1} corresponded to the D-band caused by lattice disorder of graphene and the G-band caused by the vibration in plane of sp2 hybrid carbon atoms, respectively, but the Raman bands of graphene were weak due to the lower graphene amount and the more complex components. It indicates PANI and graphene doped composites with γ-MnO_2 as the main body were successfully prepared.

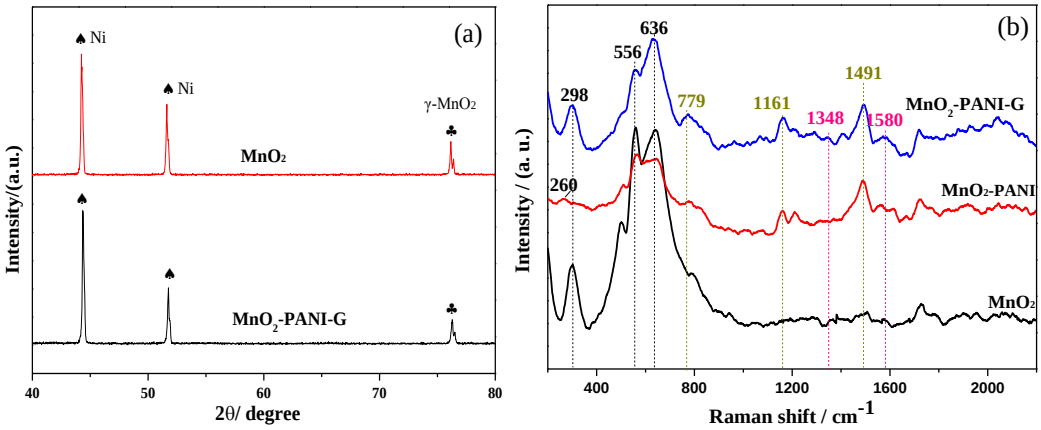

Figure 2. XRD (a) and Raman spectra (b) of different manganese dioxide electrodes

The morphologies of the nickel foam substrate, MnO_2, MnO_2-PANI and MnO_2-PANI-G electrodes are shown in Figure 3. As shown in Figure 3(a), the rough skeleton surface of nickel foam with a three-dimensional cross-linked porous structure can provide a large number of adhesion sites for the following deposition that can effectively reduce the contact and transfer resistance. The surface morphology of the MnO_2 electrode (Figure 3(b)) manifested that the surface of the nickel foam substrate was covered with a layer of MnO_2 thin film (the upper right corner inset, low-magnification imagine) and the fine grains of the surface MnO_2 film were evenly distributed and in the form of nano-crosslinking (high-magnification image), which was favorable for obtaining a large specific surface area and providing more adsorption sites. Compared with Figure 3(b), the MnO_2-PANI composite electrode presents an obvious increase in its particles size, owing to the PANI co-deposition influence, and became no longer compact and flat like the morphology of MnO_2 (Figure 3(c)), but the film became loose and its surface appeared rough. This fact suggests that PANI co-deposition may promote the nucleation process of MnO_2. As a result, MnO_2 formed more nucleation sites on the foamed nickel substrate due to PANI electrochemical co-deposition, which increased the disorder of grains and enhanced the utilization of active materials. For the MnO_2-PANI-G electrode, the MnO_2 grains, as shown in Figure 3(d), were more uniform than those in (b) and (c), and the film surface should be covered with flaked graphene.

In sum, more nucleation centers were formed and MnO_2 grains became disorder, and the surface roughness of the composite electrode was gradually increased due to adding PANI and PANI grapheme that indirectly indicated the specific surface area of the electrode was increased, which meant the adsorption performance of the composite electrode could be enhanced. Meanwhile, the composite electrode could synergistically play the role of both double-electric-layer capacitance of graphene and pseudo-capacitance of PANI, especially the addition of graphene will help to increase the solid-liquid interface contact area to make the adsorbed liquid fully infiltrate the electrode surface and to enhance the diffusion process of ions. Finally the electrode's electrical adsorption performance can be improved.

In addition, it should be noted that polyaniline doped with sulfosalicylic acid was chosen, in which hydroxyl, carboxyl, sulfo, and amine are coexist in structural chain. And graphene surface has active functional groups and π-π interaction. Thus, during the elctrodepositing, the oxygen-containing functional groups can be acted as the "interface", become the electrochemically active nucleation site, and combine with the positively charged Mn^{2+}. Once MnO_2 is formed on the surface of PANI and

graphene, which can in turn promote the degree of MnO_2 dispersion. On the other hand, because of the hydrophobicity and agglomeration of PANI and graphene as well as the usually controlled by diffusion during the co-deposition process, MnO_2 shows non-directional random nucleation, and the nuclear growth is disordered, as a result, its surface becomes roughening.

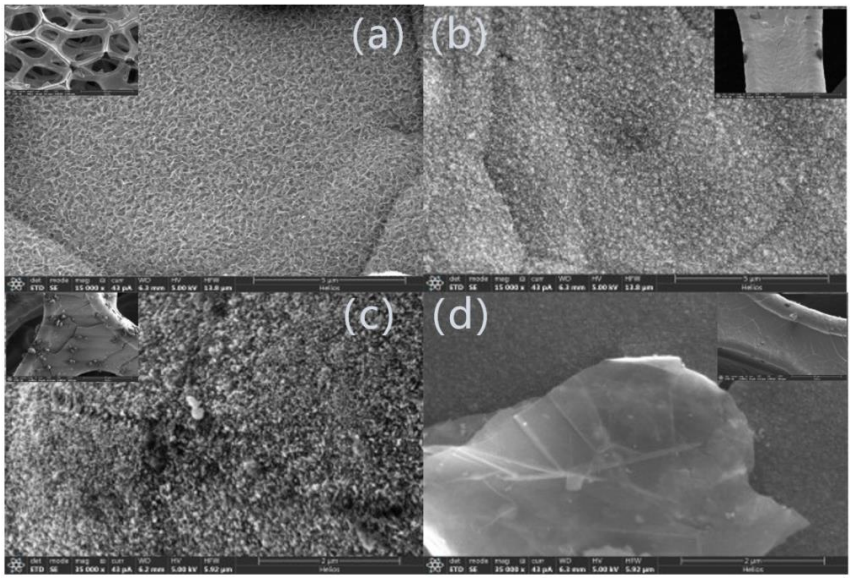

Figure 3. SEM images of (a) nickel foam substrate, (b) MnO_2, (c) MnO_2-PANI and (d) MnO_2-PANI-G electrodes

In order to further investigate the binding state of PANI, graphene and MnO_2 in the MnO_2 composite electrodes, XPS analysis was performed on the PANI powder, MnO_2-PANI and MnO_2-PANI-G composite electrodes. The XPS full spectrum of the PANI powder shown in Figure 4(a) indicated that it was composed of C, O, N and other elements. Among them, the C1s peak of PANI was fitted at 284.4, 285.5, 287.4, and 289.6 eV (Figure 4(b)), which should be assigned to C-C, C-N, C=O and O=C-O functional groups, respectively. The abundant oxygen and nitrogen functional groups in PANI will be beneficial to improve its surface polarity and thus endow certain hydrophilic properties, which are favorable for the adsorption of Pb^{2+} in the aqueous solution on the electrode surface. A detailed analysis was conducted by deconvoluting the N1s peak of PANI powder into three constituent components in Figure 4c with binding energies of 398.6, 399.9 and 401.8 eV corresponding to quinone imine (-N=), phenylcycloamino (-NH-) and positively charged diamine state imine (-NH^+=) groups, which meant PANI contained quinone and benzene rings that gave the polymer good conductivity.

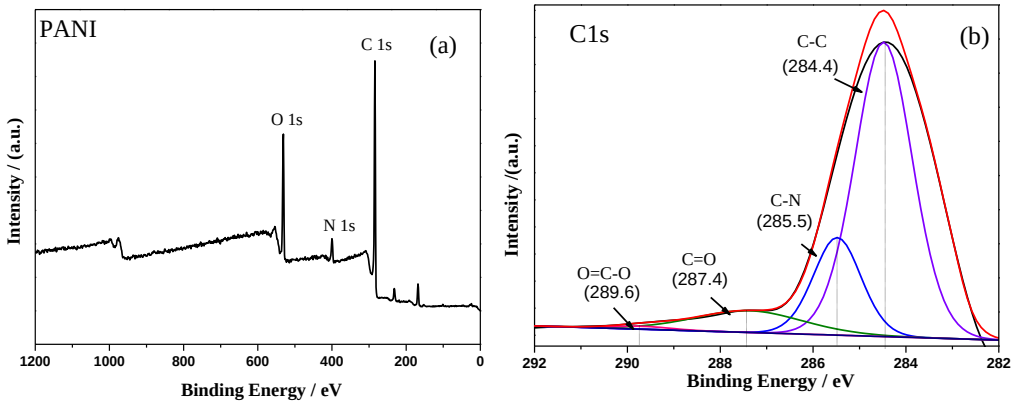

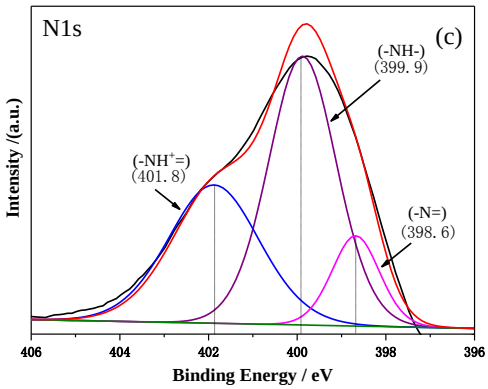

Figure 4. XPS spectrum of PANI powder (a) full spectrum, (b) C1s XPS spectrum, (c) N1s XPS spectrum

The XPS analysis results of the MnO_2-PANI electrode are displayed in Figure 5. The survey spectrum (Figure 5(a)) indicated that the film of the electrode contained Mn, C, O and N elements. This proved that PANI particles had been co-deposited and distributed in the MnO_2 film. Figure 5(b) shows the C1s spectrum. Compared to the corresponding C1s of PANI powder, the decrease of binding energy of C-C, C-N, C=O and O=C-O was more than 0.5 eV, indicating that the main chain of PANI and MnO_2 in the electrodeposition film had co-deposited by chemical bonds, and π-π conjugates and hydrogen bonds were produced between the both, and the addition of PANI probably promoted the deposition of MnO_2. The spin separation energy difference between the two main peaks of Mn2p (642.6 eV (Mn2p3/2) and 654.4 eV (Mn2p1/2) shown in Figure 5(c) is 11.8 eV, indicating that the main valence state of manganese is +4 [31,32]. Therefore, it was confirmed that the manganese oxide in the composite electrode film should be MnO_2 and the fitting of the peaks corresponded to three states of Mn^{4+}, Mn^{3+}, and Mn^{2+}, and the conversion reaction of oxidation and reduction between Mn^{4+} and Mn^{3+} improved the pseudocapacitance of MnO_2 electrode material to a certain extent, which will be beneficial to the electroadsorption reaction. In addition, the XPS spectrum of Figure 5(d) O1s is fitted to four peaks, corresponding to Mn-O (529.9 eV), -OH (531.2 eV), H-O-H (532.6 eV) and N-O bonds (533.8 eV) [33], respectively.

Figure 6(a–d) show the XPS survey spectrum and C1s, Mn2p and O1s spectra of the MnO_2-PANI-G electrode. Compared to the C1s spectra of Figures 4(b) and 5(b), it can be seen that the binding energies corresponding to C-C, C-N, C=O and O=C-O were shifted to the direction of low binding energy when graphene was involved in the electrodeposition. The energy difference between the two peaks (Mn 2p1/2 and Mn 2p3/2) for Mn2p was still 11.8 eV in Figure 6(c), indicating that the co-deposited product by adding graphene is still MnO_2. Comparing to the O1s spectrum of Figure 5(d), the binding energy of the fitted peaks of the MnO_2-PANI-G electrode obviously migrated towards the direction of low energy too. It is ascribed to the formation of more manganese-oxygen bonds lead to the increasing of lattice oxygen content in the composite film, it also shows that the chemical bond is formed between graphene and MnO_2 during the co-deposition process.

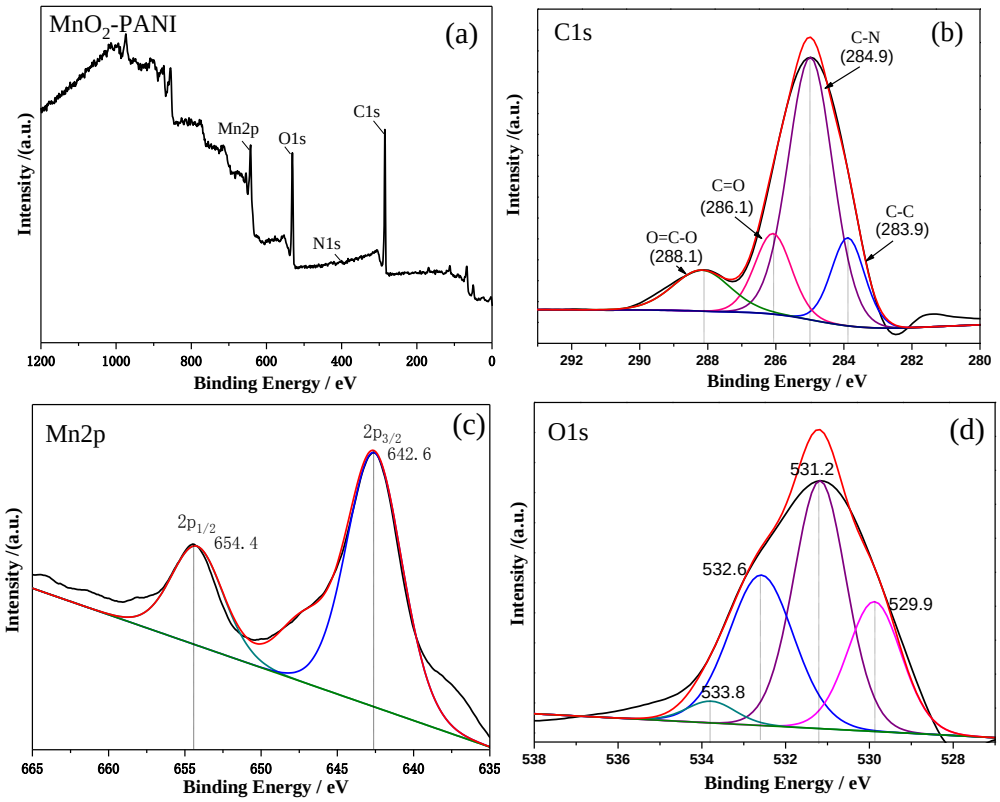

Figure 5. XPS spectrum of the MnO_2-PANI electrode (a) survey spectrum, (b) C1s XPS spectrum, (c) Mn2p XPS spectrum and (d) O1s XPS spectrum

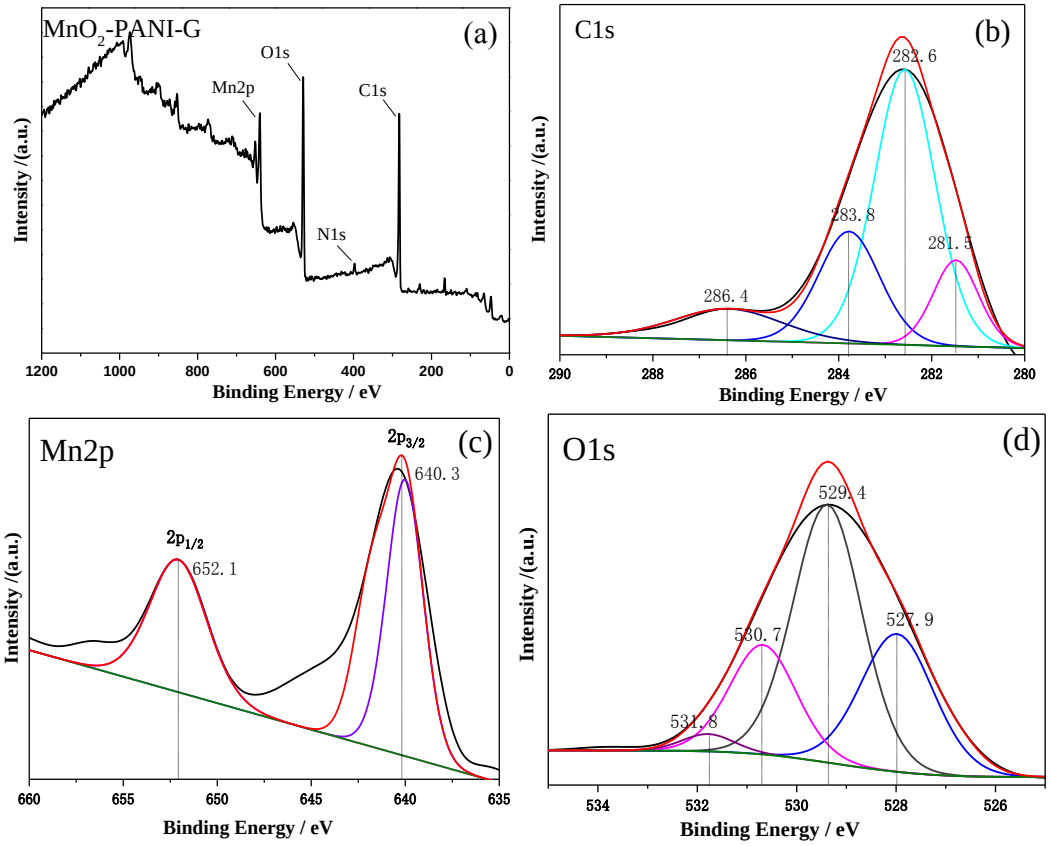

Figure 6. XPS spectrum of the MnO_2-PANI-G electrode (a) survey spectrum, (b) C1s XPS spectrum, (c) Mn2p XPS spectrum and (d) O1s XPS spectru

3.2 Capacitance characteristics of composite electrodes

The specific capacitances of different composite electrodes were measured by cyclic voltammetry (Figure 7). It can be seen that the cyclic voltammetry curves of the unmodified MnO_2 electrode and the modified composite electrodes presented good symmetrical shuttle shapes. The specific capacitances of the MnO_2 electrodes were calculated from Eq. (1) to be 29.9, 12.9, 12, and 2.9 F/g corresponding to deposition times of 1, 3, 5 and 10 min, respectively, indicating that a longer electrodeposition time led to the increase of surface resistance and the decrease of specific capacitance. The specific capacitances of the MnO_2-PANI composite electrodes were 30.3, 51.3, 37.2, and 34.8 F/g corresponding to different additions (0.5, 1, 3, and 5 g/L) of PANI in the deposition solution. The numerical variation of the specific capacitances for the MnO_2-PANI composite electrodes suggested that the addition of PANI improved the conductivity of the electrode and the synergistic effect of PANI and MnO_2 might increase the specific capacitance of the composite electrode. However, the agglomeration and encapsulation caused by the excessive PANI addition that hindered the path of electron transport and the effective utilization of material capacitance resulted in a decrease in the specific capacitance of the composite electrode. Given this, in order to make good use of adsorbing each other both PANI and graphene, and to participate in the deposition process to achieve MnO_2 composite modification, fabrication MnO_2-PANI-G composite electrodes were chosen to deposit for 1 min in the $MnSO_4$ solution including 1 g/L PANI and graphene with adding different amounts of 1, 3, 5, and 10 g/L, respectively. The corresponding specific capacitances of each composite electrode were 66.8, 132.8, 89.8, and 50.7 F/g, indicating a non-monotonic relationship of specific capacitance varying with the amount of graphene was similar to that of PANI. According to corresponding relation between MnO_2 morphology and capacitance performance via anodic electrodeposition in $MnSO_4$+H_2SO_4 solution obtained by Ye [34], the composite electrodes with MnO_2 nanosphere morphology have similar value of specific capacitance in this investigation. Compared to the CV curves of the three electrodes, it was seen the current density of MnO_2-PANI-G composite electrode increased fastest with the increase of voltage under the same conditions. The addition of PANI or/and G enhanced electrode specific capacitance value by 71.6% and 344.1% compared to that of the MnO_2 electrode due to the improvement of film conductivity Electrodes prepared by co-deposition composite had higher capacitance performance that should benefit PANI and graphene involved in the depositing process of MnO_2, promote the dispersion of MnO_2 nanostructures, increase the solid-liquid contact area of electrodes, reduce the interface resistance and improve the electrical conductivity of the composite electrodes. Simultaneously, accomplishing the composite can improve the utilization of MnO_2 and contribute to its pseudo-capacitance effect.

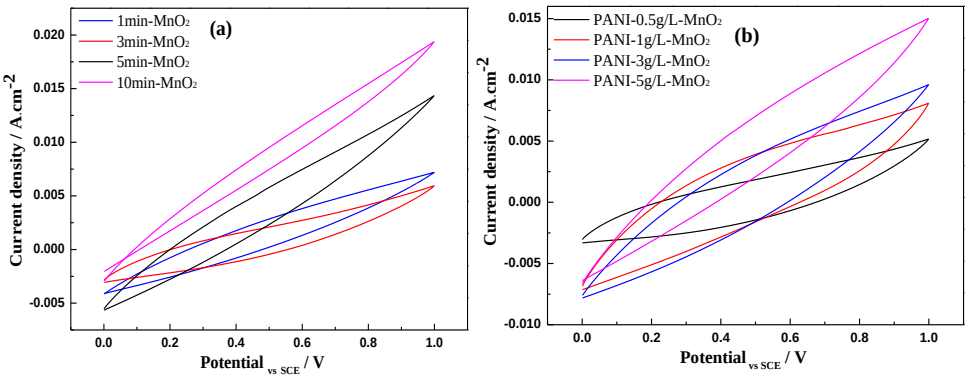

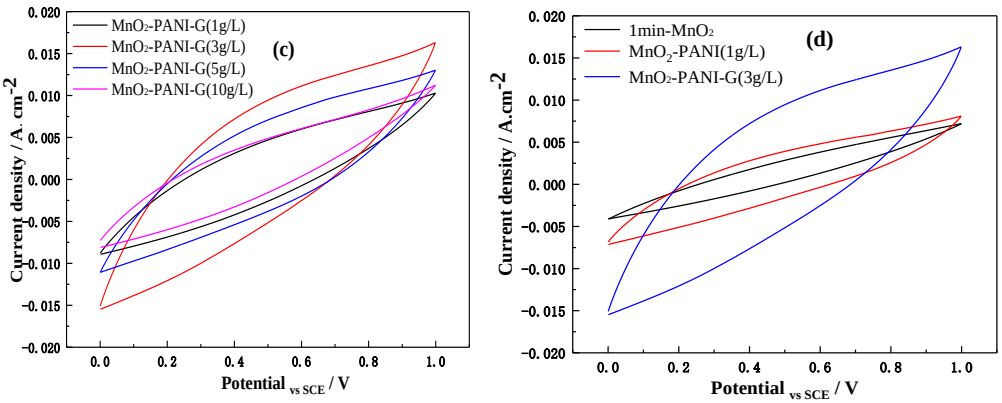

Figure 7. CV curves of different electrodes

3.3 Electroadsorption behavior of composite electrodes for Pb^{2+} ions

Figure 8(a) reveals the experimental results of the electroadsorption of different MnO_2-based composite electrodes at working voltage of 1.2 V in the lead nitrate aqueous solution with the initial conductivity of 16.23 μS/cm. It can be seen from this figure that the significant decrease of conductivity in the initial stage (within 0 to 40 min) corresponded to the distinct reduce of salt solution concentration in the CDI cell, which suggested rapid adsorption of Pb^{2+} ions. Subsequently at 50–60 min, the conductivity tended to be constant, indicating that adsorption equilibrium was gradually reached. In the initial stage of electroadsorption, different MnO_2-based electrode surfaces all provided a large specific surface area and there were many adsorption groups (active sites) exposed on the surface and inside of the electrodes, which were transferred and diffused to the active sites of the electrode in the electric field, so quick adsorption occurred. However, with the development of the electroadsorption process, the active sites on the electrode surface were gradually occupied by Pb^{2+}, the subsequent migration of ions was slowed due to the common ion effect and the diffusion process at the electrode interface slowed down, so the adsorption rate of each electrodes gradually slowed down until it reached the equilibrium point of electroadsorption when the conductivity of the solution did not change. The change of Pb^{2+} removal rate is exhibited in Figure 8(b). It can be seen from this figure that after 60 min of electroadsorption, the Pb^{2+} removal rates of MnO_2, MnO_2-PANI and MnO_2-PANI-G electrodes were 44.8%, 57.2%, and 61.8%, respectively, and the specific adsorption amounts reached 46.56, 67.05, and 72.95 mg/g. It can be seen that this facile method of composite electrodeposition can obtain the similar or even better adsorption performance compared to that of the researchers (Table 1), and overcome the problem of recycling these comparative adsorption materials, moreover the MnO_2-base composite electrodes can achieve repeated application. Compared with the MnO_2 electrode, the adsorption capacity of MnO_2-PANI-G and MnO_2-PANI electrodes increased by 56.68% and 44.01%, respectively. Reasons lie in that on the one hand, the functional group of the composite electrodes makes their hydrophilicity to enhance, which was beneficial to the infiltration of the solution and increased the diffusion and contact of Pb^{2+} ions in the simulated solution. On the other hand, the composite electrode might combine with the electric double layer capacitance and the pseudo-capacitance to jointly enhance the electrode capacitance performance and effectively improve the adsorption capacity, owing to the distributions of each composite component.

Table 1. Adsorption performance of Pb^{2+} on different adsorbents in recent literature

Adsorbents	Preparation method	Adsorption conditions	Adsorption capacity (mg/g)	Reference
Multi-walled carbon nanotubes/manganese oxide (MWCNTs/MnO_2)	In-situ growth	Solution:10mL 10 mg/L of lead nitrate; pH: 7.0; temp: 25 °C; adsorbent amount: 10mg; adsorption time:120min;	20	[35]

magnetic halloysite nanotubes@manganese oxide (MHNTs@MnO_2)	hydrothermal method	Solution:20mL 50 mg/L of lead nitrate; pH: 6.0; temp: 25 °C; adsorbent amount: 35mg; adsorption time:60min;	40.0	[36]
MnO_2 modified biochar-based porous hydrogel (MBCG)	free-radical polymerization method	Solution:150mL 50 mg/L of lead nitrate; pH: 4.0; temp: 25 °C; adsorbent amount:0.3g/L; adsorption time:1200min;	59.61	[37]
Mg–Al layered double hydroxides/MnO_2 (Mg–Al LDHs/MnO_2)	one-pot hydrothermal method	Solution:50mL 20 mg/L of lead nitrate; pH: 4.0; temp: 25 °C; adsorbent amount:50mg; adsorption time:1440min;	49.87	[38]
β-MnO_2	hydrothermal method	Solution: 10 mg/L of lead nitrate; pH: 5.5; temp: 25 °C; Pb^{2+} stock solution; adsorption time:1440min;	13.57	[39]
Al_2O_3 pillared layered MnO_2 (p-MnO_2)	Template method	Solution:500mL 80 mg/L of lead nitrate; pH: 4.0; temp: 25 °C; adsorbent amount:250mg; adsorption time:500min;	80.22	[40]
MnO_2-PANI-G	Electrodeposition	Solution:100mL 20 mg/L of lead nitrate; pH: 7.0; temp: 25 °C; adsorbent amount: 17.4mg; adsorption time:60min;	72.95	This work

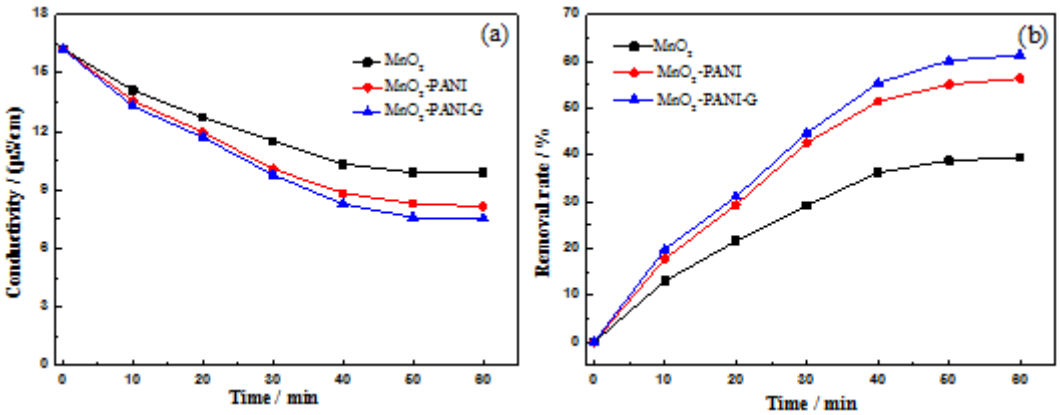

Figure 8. Electrosorption behavior of Pb^{2+} by different MnO_2-based electrodes

The quasi first-order kinetic equation (Eq. (4)) and the quasi second-order kinetic equation (Eq. (5)) were used to fit the adsorption kinetics of Pb^{2+} on different MnO_2-based capacitive film electrodes.

$$In(q_e - q_t) = Inq_e - k_1 t \quad (4)$$

$$\frac{t}{q_t} = \frac{1}{k_2 q_e^2} + \frac{t}{q_e} \quad (5)$$

where q_e is the adsorption equilibrium adsorption capacity (mg/g), q_t is the adsorption capacity at the time of T (mg/g), k_1 is the quasi first-order rate constant and k_2 is the quasi second-order rate constant.

The corresponding fitting results are shown in Figure 9 and the appropriated fitting parameters are listed in Table 2. Judged by the R^2 value, the second-order rate equation of Lagergren can well describe the adsorption kinetics of Pb^{2+}. It meant that the electroadsorption of Pb^{2+} on electrode might involve a series of processes, such as surface adsorption, diffusion in membrane and chemical adsorption. It might speculate that the adsorption process is mainly controlled by chemical adsorption [41].

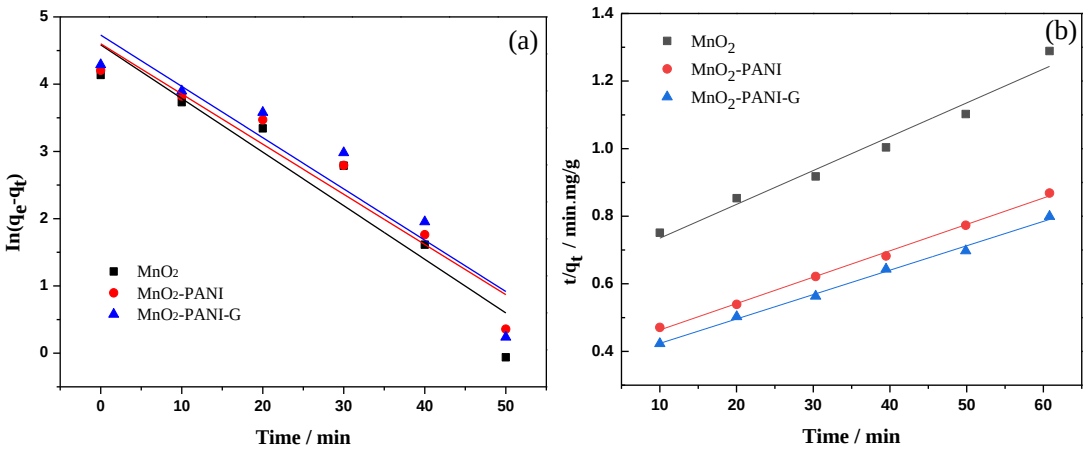

Figure 9. Fitting results of Lagergren pseudo-first (a) and pseudo-second (b) kinetic equation

Table 2. Fitting parameters of Lagergren pseudo-first (a) and pseudo-second (b) kinetic equation

electrodes	Lagergren pseudo-first			Lagergren pseudo-second		
	q_e	k_1	R^2	q_e	K_2	R^2
MnO_2	46.56	0.0797	0.9052	46.56	0.010	0.9739
MnO_2-PANI	67.05	0.0746	0.9279	67.05	0.0078	0.9975
MnO_2-PANI-G	72.95	0.0763	0.8973	72.95	0.0072	0.9955

The cycle stability comparison of three types MnO_2-based electrodes for the adsorption of Pb^{2+} is displayed in Figure 10. Experimental results revealed that the removal rate on MnO_2-PANI-G, MnO_2-PANI and MnO_2 electrodes for Pb^{2+} ion decreased by 20.7, 23.5 and 30.5% after three times of adsorption and desorption cycles. The removal rate of MnO_2-PANI-G electrode was still the highest (41.1%) after three cycles of adsorption and desorption process, indicating the composite electrode is suit for application for longer time. All the above-mentioned experimental facts presented that PANI and G were used to modify MnO_2 film electrodes by means of electrochemical co-deposition technique, which not only significantly reduced the grain accumulation of MnO_2 during the electrodeposition process to enhance the electrochemical performance of the electrode material, but also enabled to endow more functional groups on the surface of the composite material to strengthen the adsorption capacity. On the other hand, the combination of MnO_2 nanoparticles with PANI and graphene enhanced the regeneration efficiency of the composite electrode, and it stemmed from the excellent ion transport channels and more adsorption sites.

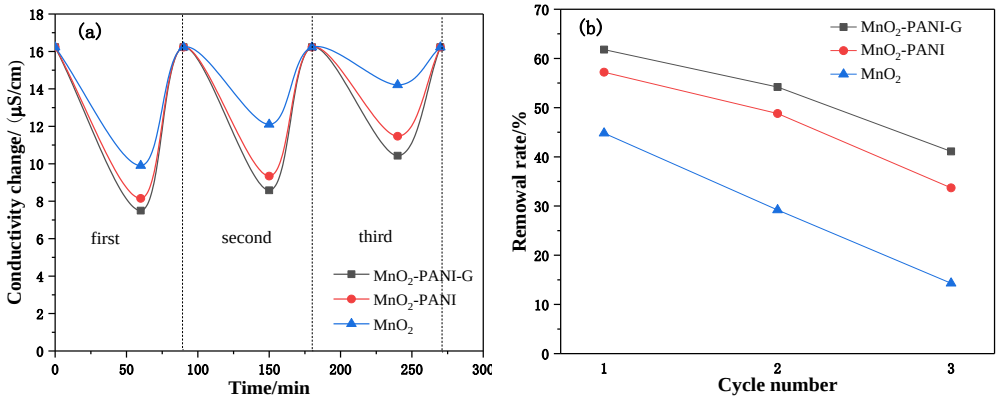

Figure 10. Cyclic stability of electrosorption of Pb^{2+} by different MnO_2-based electrodes

4.Conclusions

(1) MnO_2-PANI-G composite electrode materials with a high specific capacitance of 132.8 F/g were facilely fabricated via an anodic electrochemical co-deposition method on a nickel foam surface in a 0.1 M $MnSO_4$ solution according to the optimum process parameters: temperature 30°C; current density 1 mA/cm^2; additions of polyaniline at 1 g/L and graphene at 3 g/L.

(2) The MnO_2-PANI-G composite electrodes effectively removed 20 mg/L Pb^{2+} in the simulated solution. The adsorption equilibrium was reached after ~60 min and the Pb^{2+} ion removal rate was 61.8%. The electroadsorption process conformed to the Lagergren quasi-second-order kinetic equation. After three adsorption/desorption cycles, the electroadsorption removal rate still remained at 41.1%. The addition of PANI and grapheme also helped to enhance the regeneration and adsorption capacity of MnO_2 capacitive electrode materials.

Acknowledgements. This work was supported by the National Natural Science Foundation of China (No. 51874227) and the Natural Science basic research plan in Shaanxi province of China (Nos. 2018JM5131 and 2018JM5139).

References

1.DANIELA C. CULITA, CLAUDIA MARIA SIMONESCU, RODICA ELENA PATESCU, *et al*. Chitosan-based magnetic composites-efficient adsorbents for removal of Pb(II) and Cu(II) from aqueous mono and bicomponent solutions[J]. *Rev. Chim.*, **69**(9), 2018, 2323-2330.
2.SIMONESCU CM, CULITA DC, MARINESCU V, *et al*. Hydroxyapatite nanoparticles for acidic mine waters remediation [J], *Rev. Chim*., **70**(9), 2019, 3167-3175.
3.GRADINARU AC, SOLCAN G, SPATARU MC, *et al*. The ecotoxicology of heavy metals from various anthropogenic sources and pathways for their bioremediation [J]. *Rev. Chim.*, **70**(7), 2019, 2556-2560.
4.MIHEE L, HAN G. C, JI-WHAN A, *et al*. Leachability of arsenic and heavy metals from mine tailings of abandoned metal mines[J]. International Journal of Environmental Research and Public Health, 2009, 6: 2866-2879.
5.HU Y, LIU X, BAI J, *et al*. Assessing heavy metal pollution in the surface soils of a region that had undergone three decades of intense industrialization and urbanization [J]. Environmental Science and Pollution Research, 2013, 20(9): 6150-6159.
6.MARIA IULIANA MARCUS, MIHAELA ANDREEA MITIU, MARIA VLAD, *et al*. Influence of different electroplating sludge types on the iron ions recovery yield[J]. *Rev. Chim.*, **69**(3), 2018, 618-620.
7.MIHAI MITULETU, MARIOARA NICOLETA FILIMON, DALIBORCA CRISTIANA VLAD, *et al*. Effect of lead toxicity on the structure and function of organs in rats[J]. *Rev. Chim.*, **70**(5), 2019, 1639-1642.
8.DORIAN GABRIEL NEIDONI, VALERIA NICORESCU, LADISLAU ANDRES, *et al*. The capacity of lemna minor L. to accumulate heavy metals (Zinc, Copper, Nickel)[J]. *Rev. Chim.,* **69**(11), 2018, 3253-3256.
9.LAURENIU TATARU, VALENTIN NEDEFF, NARCIS BARSAN, *et al*. Studies of humic acid removal from aqueous systems by using polymeric membrane ultrafiltration process[J]. *Mater. Plast.*, **55**(4), 2018, 680-685.
10.STEFAN CATALIN PINTILIE, LAURENTIA GEANINA TIRON, IULIAN GABRIEL BIRSAN, *et al*. Influence of ZnO nanoparticle size and concentration on the polysulfone membrane performance[J]. *Mater. Plast*., **54**(2), 2017, 257-261.
11.LAURENTIA GEANINA TIRON, STEFAN CATALIN PINTILIE, ANDREEA LILIANA LAZAR, *et al*. Influence of polymer concentration on membrane performance in wastewater treatment [J]. *Mater. Plast.,* **55**(1), 2018, 95-98.

12.QU Y, CAMPBELL P G, HEMMATIFAR A, *et al*. Charging and transport dynamics of a flow-through electrode capacitive deionization system[J]. The Journal of Physical Chemistry B, 2018, 122:240-249.
13.Zhang Y J, Xue J Q, Li F, *et al*. Preparation of polypyrrole/chitosan/carbon nanotube composite nano-electrode and application to capacitive deionization process for removing Cu^{2+}[J]. Chemical Engineering and Processing: Process Intensification, 2019, 139:121-129.
14.JIMOH O, JERINA Z, ABDUL H, *et al*. A Comprehensive review on recently developed carbon based nanocomposites for capacitive deionization: from theory to practice[J]. Separation and Purification Technology, 2018, 207: 291-320.
15.SUN L, ZHANG C, LI J, *et al*. Assessing the sustainability of lead utilization in China[J]. Journal of Environmental Management, 2016, 183: 275-279.
16.FENG X H, ZHAI L M, TAN W F, *et al*. Adsorption and redox reactions of heavy metals on synthesized Mn oxide minerals[J]. Environmental Pollution, 2007, 147(2): 366-373.
17.EL-DEEN A G, BARAKAT N A M, KIM H Y. Graphene wrapped MnO_2-nanostructures as effective and stable electrode materials for capacitive deionization desalination technology[J]. Desalination, 2014, 344: 289-298.
18.GUO W, YU C, LI S, *et al*. Strategies and insights towards the intrinsic capacitive properties of MnO_2 for supercapacitors: challenges and perspectives[J]. Nano Energy, 2018, 57: 459-472.
19.XU J, SUN Y, LU M, *et al*. Fabrication of hierarchical $MnMoO_4{\cdot}H_2O@MnO_2$ core-shell nanosheet arrays on nickel foam as an advanced electrode for asymmetric supercapacitors[J]. Chemical Engineering Journal, 2018, 334:1466-1476.
20.CABELLO G, DAVOGLIO R A. Inorganic frameworks based on bimetallic nanoparticles encapsulated in hollow MnO_2 structures[J]. Applied Catalysis B: Environmental, 2017, 218: 192-198.
21.LV Z, LUO Y, TANG Y, *et al*. Editable supercapacitors with customizable stretchability based on mechanically strengthened ultra long MnO_2 nanowire composite [J]. Advanced Materials, 2017:170453.
22.XU W, JIANG Z, YANG Q, *et al*. Approaching the lithium-manganese oxides' energy storage limit with Li_2MnO_3, nanorods for high-performance supercapacitor[J]. Nano Energy, 2018, 43:168-176.
23.FU W, ZHAO E, REN X, *et al*. Hierarchical fabric decorated with carbon Nanowire/metal oxide nanocomposites for 1.6V wearable aqueous supercapacitors[J]. Advanced Energy Materials, 2018: 1703454.
24.HANMEI J, ZEGAO W, QIAN Y, *et al*. A novel $MnO_2/Ti_3C_2T_x$ Mxene nanocomposite as high performance electrode materials for flexible supercapacitors[J]. Electrochimica Acta, 2018, 290: 695-703.
25.LIU Y H, YU T C, CHEN Y W, *et al*. Incorporating manganese dioxide in carbon nanotube-chitosan as a pseudocapacitive composite electrode for high-performance desalination[J].ACS Sustainable Chemistry & Engineering, 2017, 6(3): 3196-3205.
26.SHI W, ZHOU X, LI J, *et al*. High-performance capacitive deionization via manganese oxide-coated, vertically aligned carbon nanotubes[J]. Environmental Science & Technology Letters, 2018, 5(11): 692-700.
27.CHEN Y, WANG M, HU Y, *et al*. Poly(2-aminothiophenol)/MnO_2 hierarchical nanocables as efficient adsorbents towards heavy metal ions[J]. Materials Chemistry and Physics, 2018, 214:172-179.
28.LI X X, DENG X H, LI Q J, *et al*. Hierarchical double-shelled poly(3,4-ethylenedioxythiophene) and MnO_2 decorated Ni nanotube arrays for durable and enhanced energy storage in super-capacitors[J]. Electrochimica Acta, 2018, 264: 46-52.
29.JULIEN C, MASSOT M, BADDOUR-HADJEAN R, *et al*. Raman spectra of birnessite manganese dioxides[J]. Solid State Ionics, Diffusion & Reactions, 2003, 159(3-4): 345-356.

30.JULIEN C M, MASSOT M, POINSIGNON C. LATTICE Vibrations of Manganese Oxides: Part I. Periodic Structures[J]. Spectrochimica Acta, Part A (Molecular and Biomolecular, Spectroscopy, 2004, 60(3): 689-700.
31.SALAM, ABDEL M. Coating carbon nanotubes with crystalline manganese dioxide nanoparticles and their application for lead ions removal from model and real water[J]. Colloids and Surfaces A: Physicochemical and Engineering Aspects, 2013, 419: 69-79.
32.RAJAKUMAR K, KIRUPHA S D, SIVANESAN S, *et al*. Effective removal of heavy metal ions using Mn_2O_3 doped polyaniline nanocomposite[J]. Journal of Nanoscience and Nanotechnology, 2014, 14(4):2937-2946.
33.ZHANG J, HAN J, WANG M, *et al*. Fe_3O_4/PANI/MnO_2 core–shell hybrids as advanced adsorbents for heavy metal ions[J]. Journal of Materials Chemistry A, 2017, 5(8), 4058-4066.
34.YE Z G, LI T, MA G, *et al*. Morphology controlled MnO_2 electrodeposited on carbon fiber paper for high-performance supercapacitors[J]. Journal of power source, 2017, 351: 51-57.
35.SALAM ABDEL M . Coating carbon nanotubes with crystalline manganese dioxide nanoparticles and their application for lead ions removal from model and real water[J]. Colloids and Surfaces A: Physicochemical and Engineering Aspects, 2013, 419: 69-79.
36.AFZALI D, FAYAZI M. Deposition of MnO_2 nanoparticles on the magnetic halloysite nanotubes by hydrothermal method for lead(II) removal from aqueous solutions[J]. Journal of the Taiwan Institute of Chemical Engineers, 2016, 63: 421-429.
37.WU Z Y, CHEN X X, YUAN B L, *et al*. A facile foaming-polymerization strategy to prepare 3D MnO_2 modified biochar-based porous hydrogels for efficient removal of Cd(II) and Pb(II)[J]. Chemosphere, 2020, 239: 124745.
38.BO L F, LI Q R, WANG Y H, *et al*. One-pot hydrothermal synthesis of thrust spherical Mg-Al layered double hydroxides/MnO_2 and adsorption for Pb(II) from aqueous solutions[J]. Journal of Environmental Chemical Engineering, 2015, 3(3):1468-1475.
39.ZHAO D.,YANG X, ZHANG H, *et al*. Effect of environmental conditions on Pb(II) adsorption on β- MnO_2 [J]. Chemical Engineering Journal, 2010, 164(1): 49-55.
40.ZHANG H, GU L, ZHANG L, *et al*. Removal of aqueous Pb(II) by adsorption on Al_2O_3-pillared layered MnO_2[J]. Applied Surface Science, 2017, 406: 330-338.
41. HO Y S, MCKAY G. Pseudo-second order model for sorption processes[J]. Process biochemistry, 1999, 34(5):451-465

Manuscript received : 02.02.2020